Oscillatory patterns composed of the parametrically excited surface-wave solitons

Xinlong Wang, and Rongjue Wei
Institute of Acoustics, Nanjing University, Nanjing 210093, People's Republic of China
(Received 2 September 1997; revised manuscript received 14 October 1997)

Multiple solitons in a water trough resonator are observed to organize into some ordered and symmetrical one-dimensional patterns that can exhibit spatiotemporal oscillations at certain excitations of the system. Experimental details including the ordering rules for the generations of stable multisoliton chains are described, and the phenomena are numerically simulated with the parametrically driven, damped nonlinear Schrödinger equation. [S1063-651X(98)15302-3]

PACS number(s): 42.65.Tg, 47.35.+i, 47.20.Ky, 43.25.+y

I. INTRODUCTION

The study of the parametrically excited surface-wave solitons in Faraday's water trough resonator [1,2] has been of fundamental importance for understanding similar or virtually the same localized phenomena recently uncovered in many other vertically driven systems of various physical media [3], such as on the interface between two fluids [4], in nonlinear lattices [5,6], in ferromagnets and antiferromagnets [7], and even in (one-dimensional [8] and 2D [9]) granular materials. So far, the stability and bifurcation behavior of a single soliton is well studied [3,10–12]. In our earlier work [13,14], we explored the dynamics of soliton-soliton interactions for some simple cases, and revealed several dynamical modes (I, II, and III). We also mentioned there [14] that these basic modes exist in many multisoliton states. However, the situations become much more complicated and yet remain to be understood when multiple solitons (number $n>2$) are strongly coupled together in a bounded channel, especially for the case when the trough length l is comparable to $n\lambda$, where λ is the extent of one solitary wave envelope. Based on our previous works [14], here we emphasize the *many body problem* and attempt to supply a clear physical picture for the general behaviors of the parametrically excited multisolitons.

In the following section (II), we shall report our recent experimental observations on the dynamics of multisolitons. Our major results include (i) the ordering rules governing the stabilities of multisoliton chains, (ii) the generic solitary-wave patterns allowed by the rules, (iii) the interesting spatiotemporal oscillations of these patterns, and (iv) the degeneration and bifurcation behaviors of the oscillatory patterns under the control of the driving parameters. In Sec. III we give some detailed descriptions and interpretations of these interesting phenomena with the *parametrically driven, damped nonlinear Schrödinger* (PDNLS) equation. Finally, in Sec. IV, we give some remarks and conclusions about the laboratory and computer experiments.

II. EXPERIMENTAL OBSERVATIONS

The solitons in a long water channel appear as some excitations highly localized in the x (longitudinal) direction, ''sloshing'' in the y (transverse) direction [1]. As before [14], we denote the polaronlike localized objects by the up and down arrows, ''↑'' and ''↓,'' and reference to a multisoliton state by the combinations of the symbols, e.g., $S(\uparrow\downarrow)$ stands for the state of two opposite polarity solitons, $S(\uparrow\uparrow)$ for a pair of like polarity solitons, etc. In the present experiment, we use a Plexiglas trough about 2.5 cm wide, filled with water to a depth of about 2.0 cm, and subjected to a vertical vibration of the form $z_0=(g/\omega^2)\Gamma\cos(4\pi ft)$. Here the driving strength Γ is normalized to the gravitational constant g, and the frequency $f=\omega/2\pi$ is adjusted to be little lower than $f_{01}\sim 5.55$ Hz [1], the linear eigenfrequency of the dominant transverse mode (0,1). In such a configuration, λ usually takes a value of about 6 cm. To produce n solitons with desired polarity arrangement, we repeatedly adjust (Γ,f) and, at the same time, apply a proper disturbance on the water surface, until the state is stabilized.

Using this setup, we have investigated various states of different polarity arrangements, with n up to 6. Among them, we observe that a state with more than two abutting solitons of like polarity appears to be unstable anyhow. These states include $S(\uparrow\uparrow\uparrow)$, $S(\uparrow\uparrow\uparrow\downarrow)$, and $S(\uparrow\downarrow\downarrow\uparrow)$, etc. For example, after the formation of $S(\uparrow\uparrow\uparrow)$ in the trough of $l\sim 30$ cm, the middle soliton is soon coalesced by one of its neighbors and thus the state transits to a bound state: $S(\uparrow\uparrow\uparrow)\Rightarrow S(\uparrow\uparrow)$, or even the state is simply replaced by other waveforms. The instability can be understood as being *due to the competitive attractions among the identical solitons.*

We find that the following states can be easily formed and sustained in some large driving parameter ranges

Type 1: $S(\uparrow\downarrow), S(\uparrow\downarrow\downarrow\uparrow), S(\uparrow\downarrow\downarrow\uparrow\uparrow\downarrow)$,

Type 2: $S(\uparrow\uparrow), S(\uparrow\uparrow\downarrow), S(\uparrow\uparrow\downarrow\downarrow)$,

$S(\uparrow\uparrow\downarrow\downarrow\uparrow), S(\uparrow\uparrow\downarrow\downarrow\uparrow\uparrow)$.

[The simplest cases $S(\uparrow\uparrow)$ and $S(\uparrow\downarrow)$ have already been well studied in our early work [13,14]. The basic experimental evidence of $S(\uparrow\downarrow\downarrow\uparrow)$ was also mentioned in [14].] What particularly interests us for these states is the synchronous spatiotemporal oscillations. (The results are recorded by video, and the copies of the records are available to interested readers upon request.) In other words, for each of these states, (i) individuals can be oscillating along the channel for some properly adjusted (Γ,f), and (ii) even if we disturb the motions out of the steps, they will soon become synchronized. Figure 1 illustrates some typical cases. As we see, the oscillating patterns can be considered simple combinations

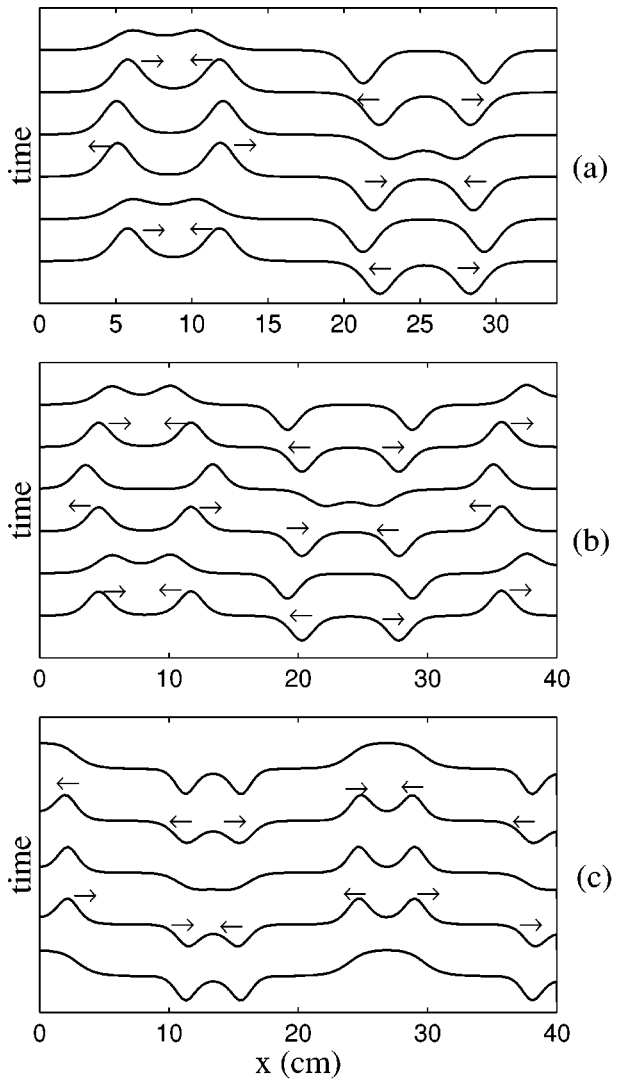

FIG. 1. Oscillations of solitary-wave chains: (a) $S(\uparrow\uparrow\downarrow\downarrow)$ ($\Gamma=0.11$, $f=5.45$ Hz), (b) $S(\uparrow\uparrow\downarrow\downarrow\uparrow)$ ($\Gamma=0.1218$, $f=5.45$ Hz), and (c) $S(\uparrow\downarrow\downarrow\uparrow\uparrow\downarrow)$ ($\Gamma=0.1551$, $f=5.50$ Hz).

of the behavior of the simplest cases $S(\uparrow\uparrow)$ and $S(\uparrow\downarrow)$ [14]. Obviously, the harmonic oscillations show the corporative behavior among the individuals. Depending on the control parameters, the oscillation frequency varies from 0.1 to 0.5 Hz.

The stabilities and the cooporative behaviors of the two stable types reflect the orders and symmetries in their structures. By applying the ''mirror effect'' [13], we see that type 1 substantiates the general pattern in an infinite waveguide:

$$\cdots\uparrow\downarrow\downarrow\uparrow\uparrow\downarrow\downarrow\uparrow\uparrow\downarrow\downarrow\uparrow\uparrow\downarrow\downarrow\uparrow\uparrow\downarrow\cdots, \tag{1}$$

which were solely composed of like pairs, with their polarity alternately distributed along the guide. At first sight, it seems that the states of type 2 would become unstable, for the same unfavorable situations as found in $S(\uparrow\uparrow\uparrow)$ would also exist if the ''mirror effect'' is applied. But here we should take notice of the inevitable existence of the viscous boundary layer or/and the surface pinning effect at the end walls. These effects, no matter how small, will spoil the ''mirror effect'' to some degree and tend to keep the solitons away from the boundaries, thus keeping the states stable. (In the states of type 1, the same effects on the solitons by the end walls are negligible, as compared to the repulsion from the neighboring solitons of opposite polarity.) The suggestion is further supported by the fact that putting a little damping material such as cotton on the end walls will make $S(\uparrow\uparrow\downarrow\downarrow)$ much more stable. We therefore draw from type 2 another general pattern:

$$\underline{\triangleright}\uparrow\uparrow\downarrow\downarrow\uparrow\uparrow\downarrow\downarrow\cdots\uparrow\uparrow\downarrow\downarrow\uparrow\uparrow\downarrow\downarrow\underline{\triangleleft}, \tag{2}$$

where the symbols ''$\underline{\triangleright}$'' and ''$\underline{\triangleleft}$'' mean the damping end walls. In a sense, this pattern can be regarded as a truncated form of the infinite one (1).

For each state of type 1 and 2, the spatiotemporal oscillation diminishes with Γ increased gradually, and individuals all become standing. On the other hand, as Γ is decreased to a certain value, one of the like pairs collapses and the pair combines into a single one, leading to the degeneration to one of the following states.

Type 3: $S(\uparrow\downarrow\uparrow), S(\uparrow\uparrow\downarrow\uparrow), S(\uparrow\downarrow\uparrow\downarrow), S(\uparrow\uparrow\downarrow\uparrow\uparrow), \ldots.$

However, the reverse process, such as $S(\uparrow\downarrow\uparrow)\Rightarrow S(\uparrow\downarrow\downarrow\uparrow)$, is seldom observed, which shows the hysteresis in the real system. The threshold of the degeneration depends on the driving frequency f and the trough dimension as well. For instance, in the trough of $l=34$ cm, $S(\uparrow\downarrow\downarrow\uparrow)\Rightarrow S(\uparrow\downarrow\uparrow)$ when Γ is decreased to 0.101 at $f=5.45$ Hz, while at $f=5.5$ Hz, this happens at $\Gamma=0.094$. Of course, each state of type 3 can be produced directly; each can also exhibit the spatiotemporal oscillation, but the situations are somewhat more sophisticated. For example, depending on (Γ,f), the solitons in $S(\uparrow\downarrow\uparrow)$may oscillate either as

$$S(\overrightarrow{\uparrow}\downarrow\overleftarrow{\uparrow}),\ S(\overrightarrow{\uparrow}\downarrow\overleftarrow{\uparrow}),\ldots,$$

or

$$S(\overleftarrow{\uparrow}\overleftarrow{\downarrow}\overleftarrow{\uparrow}),\ S(\overrightarrow{\uparrow}\overrightarrow{\downarrow}\overrightarrow{\uparrow}),\ldots,$$

where ''$\rightarrow$ '' and ''$\leftarrow$'' denote the directions of motions.

In principle, more than 6 solitons could also be formed in the water trough. However, it becomes much more difficult in experiment to manually supply a proper initial surface waveform, e.g., a sudden disturbance on the water surface, which would definitely evolve into what we desire ($n>6$). Moreover, additional difficulty also arises in generating such a multisoliton chain, for the unwanted excitations of longitudinal waves usually become unavoidable in a very long trough (note that $l\sim n\lambda$). In spite of these, it is straightforward to generalize the above observed results to the case of $n>6$.

III. NUMERICAL SIMULATIONS

Now we attempt to interpret and describe what we have observed with the PDNLS equation

$$i(\phi_\tau+\alpha\phi)+\phi_{XX}+2|\phi|^2\phi+\beta\phi+\gamma\phi^*=0, \tag{3}$$

where ϕ is the solitary-wave envelope modulating on crosswave mode (0,1), α the damping coefficient, and the asterisk denotes complex conjugate. The equation was first proposed

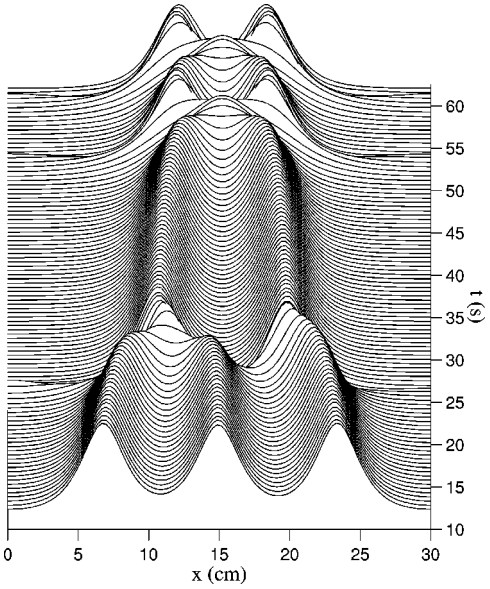

FIG. 2. The instability of $S(\uparrow\uparrow\uparrow)$ and the transition to an oscillating bound state at $(\alpha,\beta,\gamma)=(0.6455,\ -1,\ 0.9778)$.

by Miles [2] to model the parametrically excited solitary-wave phenomena in an unbounded channel. For the details as well as the incorporation of the surface tension effect, we refer readers to Miles's contribution. The relations of the variables and parameters in Eq. (3) to those used in the experiment are described below in brief. Let ϵ be a small parameter $(0<\epsilon\ll 1)$ that measures the strength of nonlinearity. Then,

$$\beta\equiv\frac{f^2-f_{01}^2}{2\epsilon f_{01}^2},\quad \gamma\equiv\frac{\Gamma}{\epsilon},\tag{4}$$

and ϕ is a function of the slow variables (X,τ), respectively defined as

$$X=2\sqrt{\epsilon}\sqrt{\frac{T}{T+kh(1-T^2)}}kx,\quad \tau=\epsilon\omega t,\tag{5}$$

where $T\equiv\tanh(\pi h/b)$, $\omega=2\pi f$, b is the breadth of the water trough, and h is the height of water. In what follows, we assume

$$\epsilon=-\frac{f^2-f_{01}^2}{2f_{01}^2}>0,\tag{6}$$

so that $|\beta|$ is normalized to unity. Our derivation by using a multiple scales' method shows that Eq. (3) is still valid for *the present case of the bounded channel*, if letting

$$\beta=-1-\nu\langle|\phi|^2\rangle,\tag{7}$$

where $\langle\cdot\rangle$ denotes the average over the channel and

$$\nu\equiv\frac{8(1-T^2)^2}{(6T^4-5T^2+16-9T^{-2})}.$$

The modification is required by the mass conservation of fluid [15] in the bounded container. In our experiments, $T\simeq 0.987$ and $\nu\simeq 7\times 10^{-4}$, so it is insignificant and negligible. To numerically solve Eq. (3), together with the rigid boundary condition $\phi_x=0$ at the end walls $x=0$ and l, we use the same algorithm as ours before [14]. We first apply

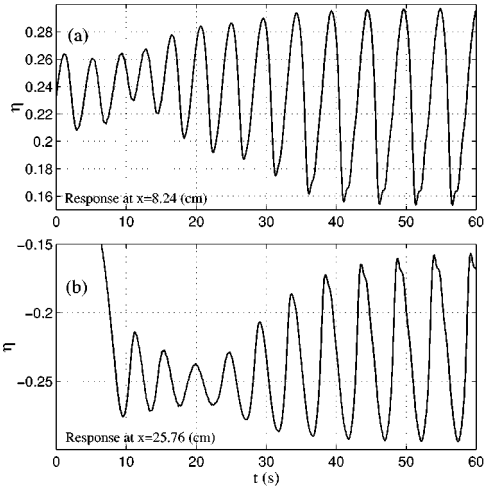

FIG. 3. Synchronization of the two oscillating bound pairs in $S(\uparrow\uparrow\downarrow\downarrow)$ $[\eta=\mathrm{Im}(\phi)]$. [Parameters: $l=34$ cm, $(\alpha,\gamma)=(0.6,\ 0.9903)$, and $C=20$ at $x=0,l$.]

the implicit finite difference algorithm with respect to X, so that Eq. (3) becomes a set of discrete ordinary differential equations for $\phi^{(n)}\equiv\phi(X_n,\tau)$

$$i(\phi_\tau^{(n)}+\alpha\phi^{(n)})+\frac{1}{h_X^2}(\phi^{(n+1)}-2\phi^{(n)}+\phi^{(n-1)})$$
$$+2|\phi^{(n)}|^2\phi^{(n)}+\beta\phi^{(n)}+\gamma(\phi^{(n)})^*=0,$$
$$(n=0,1,2,\ldots,N-1),\tag{8}$$

with the boundary condition

$$\phi^{(-1)}=\phi^{(1)},\quad \phi^{(N)}=\phi^{(N-2)},\tag{9}$$

at X_0 and X_{N-1}, where $X_n=nh_X$, $h_X=L/(N-1)$, N is the number of differencing points, and the dimensionless system interval L is related to the trough length l through (5). We then integrate Eqs. (8) in time τ by the *Runge-Kutta-Fehlberg* algorithm. In the computations, numerical error is controlled within 10^{-6}.

Numerically we investigate a multisoliton chain by locating its control parameter region of stability on the (α,γ) plane. We only consider the parameter ranges usually used in the experiment. We find out that such a region does not exist for the states that have *more than two like polarity individuals neighboring each other*. A typical case is the three identical soliton state $S(\uparrow\uparrow\uparrow)$, which is observed to be unstable in experiment. Figure 2 shows how, in a trough of $l=30$ cm, these identical solitons interact with each other, and then, evolve into an oscillating bound state $S(\uparrow\uparrow)$, i.e., $S(\uparrow\uparrow\uparrow)\Rightarrow S(\uparrow\uparrow)$. Initially the three solitons are positioned, respectively, at $x=6.8$, 15, and 23.5 cm. At $t\sim 25$ s, the two solitons of smaller separation (here the first and the second solitons) combine into a single one, due to the stronger attraction in between. [Note that, for the given initial waveform, the solitons are much closer to each other than to their virtual images (due to mirror effect of rigid boundary condition), so the influence of two end wall boundaries are comparatively small.] The similar situations have also been found in the simulations to the other states such as

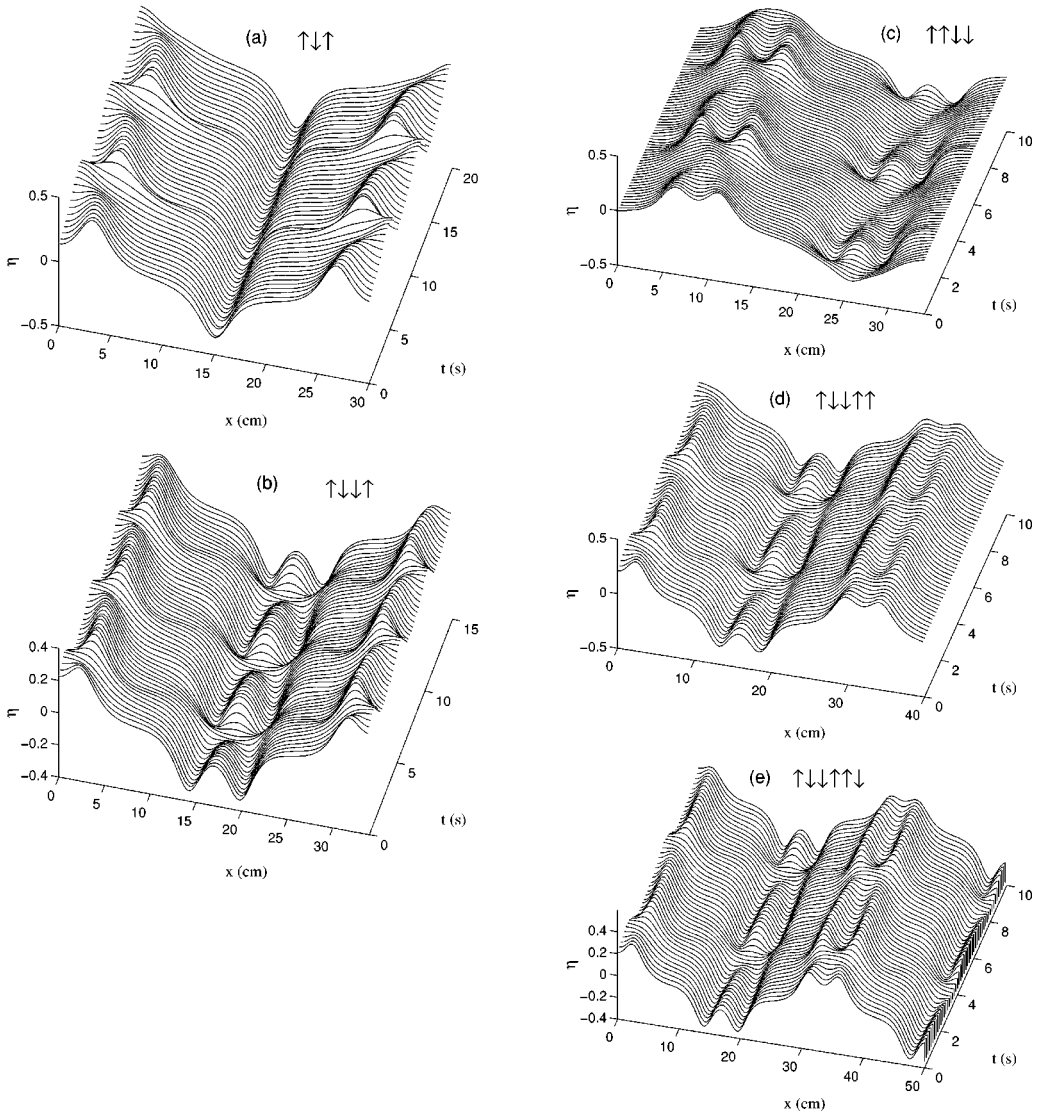

FIG. 4. Simulations of the time evolutions of the oscillatory patterns [$\eta = \mathrm{Im}(\phi)$]. (a) $S(\uparrow\downarrow\uparrow)$ at $(\alpha,\gamma)=(0.6455,\ 0.9778)$, (b) $S(\uparrow\downarrow\downarrow\uparrow)$ at $(\alpha,\gamma)=(0.9445,\ 1.2976)$, labeled by ''$\oplus$'' in Fig. 5(a); (c) $S(\uparrow\uparrow\downarrow\downarrow)$ at $(\alpha,\gamma)=(0.8938,\ 1.2326)$ ($C=\infty$ at $X=0,L$); (d) $S(\uparrow\downarrow\downarrow\uparrow\uparrow)$ at $(\alpha,\gamma)=(0.6003,\ 1.0512)$ ($C=\infty$ at $X=L$); (e) $S(\uparrow\downarrow\downarrow\uparrow\uparrow\downarrow)$ at $(\alpha,\gamma)=(0.6003,\ 1.0446)$ labeled by ''$\otimes$'' in Fig. 5(a). (Note that $C=\infty$ means a highly damping boundary.)

$S(\uparrow\downarrow\downarrow\downarrow\uparrow)\Rightarrow S(\uparrow\downarrow\downarrow\uparrow)$ and $S(\uparrow\downarrow\downarrow\downarrow\downarrow\uparrow)\Rightarrow S(\uparrow\downarrow\downarrow\uparrow)$. Therefore, the numerical simulations have confirmed the experimental observations of the instability of the states with more than two neighboring like solitons.

Before presenting the details of the numerical results for the three stable types, we point out the different treatments of the boundary condition in simulating different types. By directly using the numerical procedure and the rigid boundary condition (9) to type 1 [and some of type 3, such as $S(\uparrow\downarrow\uparrow)$ and $S(\uparrow\downarrow\uparrow\downarrow)$], we have successfully reproduced every aspect experimentally observed (see below). However, we fail to locate the stability regions for type 2 [and some other states of type 3, such as $S(\uparrow\uparrow\downarrow\uparrow)$]. In fact, if simply applying the boundary condition (9), the physical situations for type 2 [and some of type 3], say $S(\uparrow\uparrow\downarrow\downarrow)$, are essentially the same as those of the unstable states just described in the last paragraph. As a result, in the state $S(\uparrow\uparrow\downarrow\downarrow)$, for example, the solitons near the two end walls will be attracted by and then attached to the boundaries, or even $S(\uparrow\uparrow\downarrow\downarrow)\Rightarrow S(\uparrow\uparrow\downarrow)\Rightarrow S(\uparrow\downarrow)$. To interpret the stability of the type, we model the experimental situations by taking a greater damping coefficient α at the boundaries $X=X_0$ and X_{N-1} [only X_0 for $S(\uparrow\uparrow\downarrow)$ and $S(\uparrow\uparrow\downarrow\downarrow\uparrow)$] than elsewhere. This is implemented simply by replacing the damping coefficient α for the difference equations $n=0$ and $N-1$ in Eq. (8) by $C\alpha$, where $C>1$. With this treatment, everything observed for type 2 (and some of type 3) can also be well reproduced. The greater the coefficient C is, the larger the parameter region of the stability for such a state. This confirms the experimentally based suggestion about the stability of type 2.

To illustrate how the individuals get synchronized, Fig. 3 gives the responses at the centers of two bound pairs of $S(\uparrow\uparrow\downarrow\downarrow)$ when $C=20$. As is clearly seen, the two oscillating pairs are 180° phase locked after a few interacting cycles. After getting synchronized, the solitons will oscillate in a stationary pattern. Some of the examples of the simulations of the time evolutions are presented in Fig. 4, where (b) and (e) are of type 1, (c) and (d) type 2, and (a) type 3. Each of

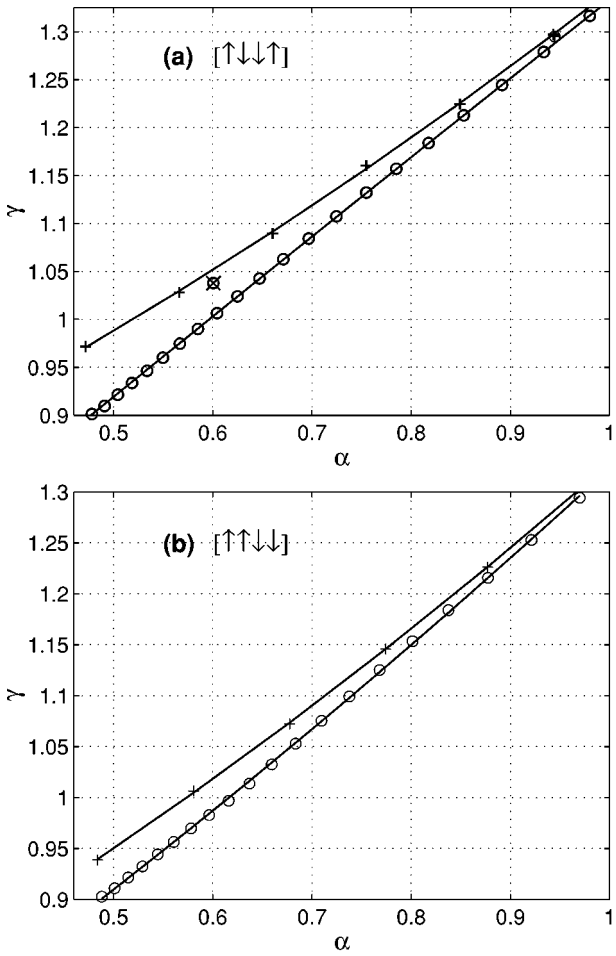

FIG. 5. Stability diagrams in the channel of $l=34$ cm. For each case, the stability domain for the oscillatory pattern lies between the upper and lower lines, which are the best fits of the computed points, ''+'' and ''○,'' respectively; below the region, the states degenerate into the ones of fewer solitons, while above the region all solitons become standing.

these oscillatory patterns has its own stability regions. Figure 5(a) is the computed stability diagram in the (α,γ) plane for the steady state $S(\uparrow\downarrow\downarrow\uparrow)$ [$S(\uparrow\downarrow)$ and $S(\uparrow\downarrow\downarrow\uparrow\uparrow\downarrow)$ have the similar ones], while (b) is the one for $S(\uparrow\uparrow\downarrow\downarrow)$ in the case of highly damping boundaries ($\alpha\rightarrow\infty$, or $\phi\simeq 0$, at $x=0$ and l). In the diagrams, the conelike bands between two lines are the parameter regions of the stationary oscillatory patterns.

As γ is decreased across the lower boundary of the stability regions, one or more bound pairs are combined into single solitons, and the states thus degenerate to the ones of fewer individuals. As a typical example, Fig. 6(a) shows how $S(\uparrow\downarrow\downarrow\uparrow)$ degenerates as γ is decreased. When $t<20$ s, γ is located inside the oscillatory parameter regions, and thus the state behaves as shown in Fig. 4(b). At the time $t=20$ s, γ is decreased to a value just below the stable region (see Fig. 5), and thus $S(\uparrow\downarrow\downarrow\uparrow)\Rightarrow S(\uparrow\downarrow\uparrow)$. Since the value of γ is relatively large for $S(\uparrow\downarrow\uparrow)$, the resulting state becomes standing. Further decrease of γ (at $t=60$ s) will have the solitons oscillate. Just as observed in experiment, the three oscillating solitons will get synchronized (in one interacting cycle), and then ($t>80$ s) they oscillate in the sequence of

$$S(\overleftarrow{\uparrow}\,\downarrow\,\overrightarrow{\uparrow})\Rightarrow S(\overrightarrow{\uparrow}\,\downarrow\,\overleftarrow{\uparrow})\Rightarrow S(\overleftarrow{\uparrow}\,\downarrow\,\overrightarrow{\uparrow})\Rightarrow S(\overrightarrow{\uparrow}\,\downarrow\,\overleftarrow{\uparrow})\Rightarrow\cdots,$$

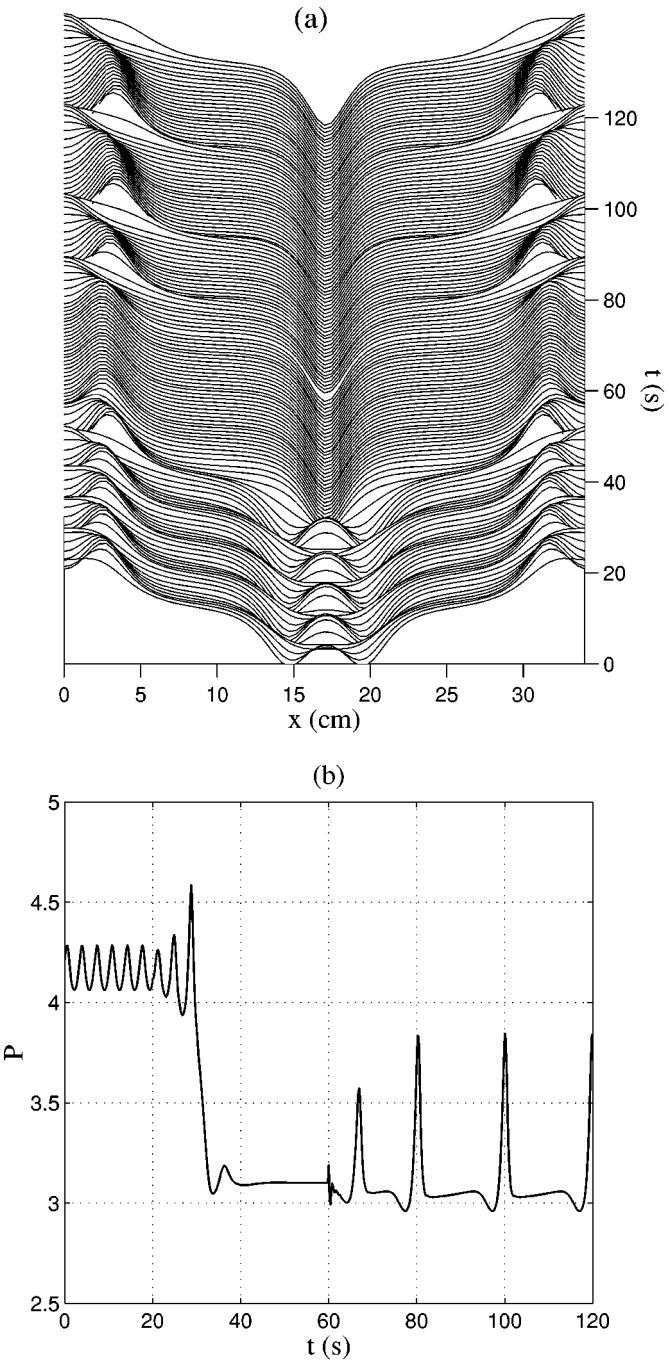

FIG. 6. Degeneration of the 4-soliton state $S(\uparrow\downarrow\downarrow\uparrow)$ at a fixed damping coefficient, $\alpha=0.9445$, in the trough of $l=34$ cm: (a) time evolution of the transitions; (b) variation of the ''particle number'' P with time. The driving strength takes the values (1) $\gamma=1.2982$ for $t<20$ s; (2) $\gamma=1.2894$ for 20 s$\leqslant t<60$ s; (3) $\gamma=1.222$ for $t\geqslant 60$ s.

while keeping the middle soliton standing, which is same as shown in Fig. 4(a). The transition process can be better characterized by the ''particle number'' $P(\tau)$ [14], as is the shown in Fig. 6(b). Here the quantity is normalized with respect to a single soliton, i.e.,

$$P(\tau)\equiv\frac{\int_0^L|\phi(X,\tau)|^2dX}{\int_{-\infty}^{\infty}|\phi_s(X)|^2dX}, \tag{10}$$

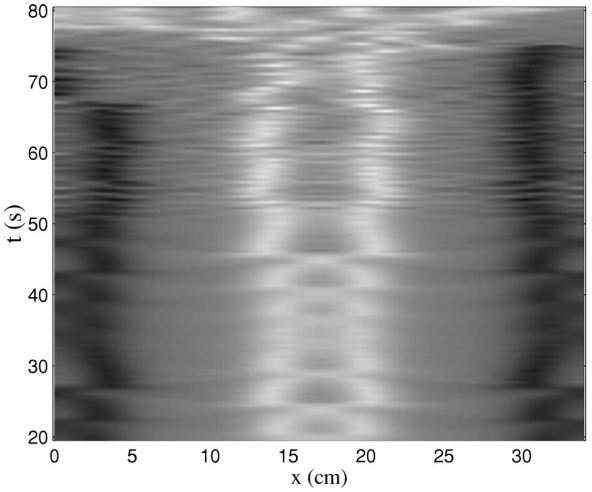

FIG. 7. Onset of spatiotemporal chaos from the 4-soliton state $S(\downarrow\uparrow\uparrow\downarrow)$ as (α,γ) changes from (0.5, 0.95) to (0.3, 0.9256) at the time $t=50$ s. The gray level is proportional to $\mathrm{Im}(\phi)$, so the darkest sites are the two solitons close to the boundaries, while the brightest ones are the two like solitons (bound pair).

where $\phi_s(X)$ is the single standing soliton solution to Eq. (3) in an unbounded channel [2]. In this definition, $P\approx n$ for an n-soliton state. For a standing state, P is a constant in time, but for an oscillating one, P varies periodically in the vicinity of n.

Finally, we mention that spatiotemporal chaos will occur to the oscillatory patterns for low dissipation, namely, $\alpha<0.5$. As α is decreased along the stability bands in Fig. 5, the oscillations first appear to be quasiperiodic temporally. Further decrease of α will give rise to the destruction of the coherent structures in space and irregular motions in time, and thus lead to the onset of spatiotemporal chaos. Figure 7 shows how the quasiperiodical oscillation of $S(\uparrow\downarrow\downarrow\uparrow)$ becomes chaotic both in time and space as (α,γ) changes from (0.5, 0.95) to (0.3, 0.9256). The numerical evidence has also been proved by our experiment at low frequency f and using very clean water. [Note that $\alpha\equiv\delta/\epsilon$ (see [2]), where δ is the ratio of actual to critical damping for free oscillation of the first transverse mode (0,1) and ϵ is given by Eq. (6). In a given experimental configuration, δ almost keeps constant, and thus lowering the driving frequency f is equivalent to decreasing damping coefficient α.] The interesting behavior indicates that, in addition to the ordering rules, dissipation plays another important role in stabilizing and supporting the parametrically excited oscillatory patterns. An in-depth investigation of the complex dynamics of the transition to spatiotemporal chaos will be given elsewhere.

IV. DISCUSSION AND CONCLUSIONS

To compare with the experiments directly, one should take notice of the difficulty to precisely determine α experimentally, as well as the high sensitivity of γ to the experimental parameters such as b, h and the surface-tension coefficient. For example, the measurement errors of b and h are about ±0.025 and ±0.05 cm, respectively, in our experiment. It immediately follows that $\gamma=1.297\pm0.226$, which almost span over the stability domains, as can be seen in Fig. 5. In spite of this, we see that Eq. (3) can describe the observed phenomena satisfactorily.

In summary, both our experimental and numerical works show that the spatial arrangement orders of the polaronlike solitons are responsible for the stabilities of the 1D parametrically excited solitary-wave chains, and the stable chains assume some very orderly and symmetric structures, which can be abstracted as two general patterns (1) and (2) (and their degenerate, type 3). Quite different from those found in other 1D systems [16,17], these patterns are solely composed of polaronlike ''molecules''—bound pairs ($\uparrow\uparrow$'s and $\downarrow\downarrow$'s)—and, in particular, the corporative interactions of the bound pairs result in the spatiotemporal oscillations of the patterns, not yet observed in the 2D analogous ''molecular'' and ''crystalline'' structures [9]. The agreement between the experiment and the numerical simulations suggests the existence of the same or similar structures in other vertically driven systems modeled by the same equation [3–7]. The approach may also provide a clue for understanding the formation and dynamics of the patterns in biological, chemical, and physical systems in general [18].

The work was supported by the National Natural Science Foundation of China (Project No. 19774029) and the State Key Laboratory of Modern Acoustics of Nanjing University.

[1] J. R. Wu, R. Keolian, and I. Rudnick, Phys. Rev. Lett. **52**, 1421 (1984).
[2] J. W. Miles, J. Fluid Mech. **148**, 451 (1984).
[3] M. Bondila, I. V. Barashenkov, and M. M. Bogdan, Physica D **87**, 314 (1995) (also see the references therein).
[4] W. Z. Chen, R. J. Wei, and B. R. Wang, Phys. Lett. A **208**, 197 (1995).
[5] B. Denardo *et al.*, Phys. Rev. Lett. **68**, 1730 (1992).
[6] W. Z. Chen, Phys. Rev. B **49**, 15 063 (1994).
[7] I. V. Barashenkov, M. M. Bogdan, and V. I. Korobov, Europhys. Lett. **15**, 113 (1991).
[8] W. Z. Chen, Phys. Lett. A **196**, 321 (1995).
[9] P. B. Umbanhowar, F. Melo, and H. L. Swinney, Nature (London) **382**, 793 (1996).
[10] E. W. Laedke and K. H. Spatchek, J. Fluid Mech. **223**, 589 (1991).
[11] H. Friedel, E. W. Laedke, and K. H. Spatschek, J. Fluid Mech. **284**, 341 (1995).
[12] W. Z. Chen, R. J. Wei, and B. R. Wang, Phys. Rev. E **53**, 6016 (1996).
[13] X. L. Wang and R. J. Wei, Phys. Lett. A **192**, 1 (1994); **227**, 55 (1997).
[14] X. L. Wang and R. J. Wei, Phys. Rev. Lett. **78**, 2744 (1997).
[15] A. Larraza and S. Putterman, J. Fluid Mech. **148**, 443 (1984).
[16] F. Melo and S. Douady, Phys. Rev. Lett. **71**, 3283 (1993).
[17] H. J. Balmforth, Annu. Rev. Fluid Mech. **27**, 337 (1995).
[18] M. C. Cross and P. C. Hohenberg, Rev. Mod. Phys. **65**, 851 (1993).